Chinese Journal of Physics 77 (2022) 1278–1290

Contents lists available at ScienceDirect

Chinese Journal of Physics

journal homepage: www.elsevier.com/locate/cjph

A numerical and statistical approach to capture the flow characteristics of Maxwell hybrid nanofluid containing copper and graphene nanoparticles

A. Bhattacharyya [a], R. Sharma [b,*], S.M. Hussain [c], A.J. Chamkha [d], E. Mamatha [b]

[a] Department of Mathematics, BMS Institute of Technology and Management, Bengaluru 560064, Karnataka, India
[b] Department of Mathematics, GITAM School of Science, GITAM University, Bengaluru 562163, Karnataka, India
[c] Department of Mathematics, Faculty of Science, Islamic University of Madinah, Madinah 42351, Saudi Arabia
[d] Faculty of Engineering, Kuwait College of Science and Technology, Doha District, 35004, Kuwait

ARTICLE INFO

Keywords:
Maxwell nanofluid
Graphene nanoparticles
Joule heating
Thermal radiation
Inclined magnetic field
Stretching sheet

ABSTRACT

The principal goal of the present investigation is to inspect the flow characteristics of an electrically conducting hybrid nanofluid containing copper and graphene nanoparticles past a linearly stretched sheet with velocity slip condition at the interface. Since, the non-Newtonian fluid models result in a better understanding of the flow and heat transfer attributes of the nanofluids, therefore, non-Newtonian Maxwell nanofluid has been chosen as the base fluid in our study with an unsteady magnetic field applied at a certain angle to the direction of the flow. Consideration of thermal radiation along with heat absorption under the mutual influence of viscous and Joule dissipations is one of the key features of this research investigation. With the help of similarity transformations, the governing flow equations have been converted into a system of coupled non-dimensional differential equations. After that, Shooting method along with Runge–Kutta–Fehlberg numerical technique is employed to find the solutions for velocity and temperature of the hybrid nanofluid. The obtained numerical results are well demonstrated with a number of graphs and tables. Apart from this numerical technique, a statistical method is implemented of multiple quadratic regression estimation analysis on the various graphs of skin friction coefficient and wall temperature gradient to establish the connection among physical entities and heat transfer rate. The applications of this investigation in solar energy, ventilation, heating as well as refrigeration , medical science, defence sector etc. Some noteworthy findings include that Maxwell parameter, velocity slip and porosity have a tendency to reduce the hybrid nanofluid velocity whereas graphene Maxwell hybrid nanofluid's temperature is getting enhanced for rising the values of magnetic field's inclination angle, radiation, unsteadiness parameters, Biot number and viscous dissipation whereas a reverse trend is visible for heat absorption parameter. Furthermore, the permeability of the porous medium has a more significant impact on changing the nanofluid velocity than that of magnetic parameter whereas the rate of heat transfer is high sensitive for thermal radiation than that of viscous dissipation. As per authors' knowledge there is no such attempt where the mutual effects of hybrid Maxwell nanofluid (graphene and copper), porous media and viscous dissipation have been considered.

* Corresponding author.
E-mail address: rohit.iitg08@gmail.com (R. Sharma).

https://doi.org/10.1016/j.cjph.2021.09.015
Received 25 May 2021; Received in revised form 13 August 2021; Accepted 5 September 2021
Available online 27 October 2021

1. Introduction

In present scenario, study of nanofluid are getting a lot of attention, due to its noteworthy applications in industries because of its boosting nature of rate of heat transfer. Choi [1] was the first scientist who noticed that a noble enhancement is occurring when non-metallic/metallic particles are mixed with fluid. Adding the extra fine particle in fluid is the reason of notable changing of fluid nature like thermal conductivity and heat transfer rate [2]. Nanofluids have a lot of applications in energy conversion, cooling of microsystem's, optical devices and sensor. Both experimental and numerical reviews were done by Rashidi et al. [3] and they expressed the significance as well as disadvantages of nanofluid in evaporating systems. Das et al. [4] studied the double diffusive natural convection flow of nanofluid over a plate which is inclined at particular angle. Seth et al. [5] analysed the entropy generation mechanism for the dissipative flow of carbon nanotubes in rotating frame with Darcy–Forchheimer porous medium. Analysing the nature of MHD stagnation point viscous nanofluid flow passing through a curved surface was carried out by Nadeem et al. [6]. Rheological influence because of oscillating field on unsteady boundary layer flow of magnetic nanofluid passing through a rotational disc has been studied by Ram et al. [7]. Rana and Nawaz [8] analysed the nature of Sutterby nanofluid and found enhancement of rate of heat transfer. Ma et al. [9] has shown the effect of geometry and Baffle on forced convection on the backward and forward steps channel, by employing of lattice Boltzmann methods. Xu et al. [10] described the optomechanical wagon-wheel effects for bidirectional sorting of dielectric nanoparticles. Zhang and Zhang [11] presented an experimental study on enhanced heat transfer and flow performance of magnetic nanofluids under alternating magnetic field.

The monomolecular layer of carbon atom which has the structure similar to that of honeycomb is known as graphene. Because of having high thermal conductivity, fast mobility of electrons and expanded surface area, the graphene nanoparticles exhibit the novel material, physical, electrical and chemical characteristics [12]. Naturally, it finds a large scale application in various electronics as well as energy sectors [13]. While performing the theoretical investigation of magneto-Carreau fluid containing the graphene and dust particles, Upadhya et al. [14] observed a significant enhancement in the heat transport phenomenon. Later, Mahesha et al. [15] extended this investigation by considering different aspects such as thermal radiation and heat generation and found a noteworthy improvement in the heat transfer mechanism. Hydromagnetic fluid flow through porous medium has some crucial applications in variety of engineering and industrial sectors which include separation of metal from non-metallic enclosures, extraction of energy from earth, polymer industries, etc. Some notable research works regarding the fluid flow through porous medium are due to [16–20].

Majority of above mentioned research articles are related to Newtonian fluids. But practical situation is quite different, many non-Newtonian fluids such as polymers, pulps, lubrication, liquid metals are frequently used in several industrial and engineering process. Due to its complicated characteristics, till no one found the single equation which can present all the nature of this types of non-Newtonian categories of fluids. Various complicated model was proposed by many investigators such as, Baris and Dokuz [21], Haroun [22], Sajid et al. [23] and Hayat et al. [24], etc. Models are related to 2nd , 3rd and 4th grade fluids which exhibit the consequences of elasticity whereas the mathematical models are not dependent on shear and not able to imagine the importance of shear relaxation [25]. Further, Maxwell model is given because it can measure relaxation of shear stress and thus construct a famous model by the several investigators. These mathematical models can also interpret the importance of viscosity problem in boundary layer. Consequently, a number of researchers such as Fetecau and Fetecau [26], Wang and Hayat [27] and Heyhyat and Khabazi [28] mentioned their investigation on Maxwell fluid flow problems under the consideration of various geometrical sketch to study the importance of various germane parameter on fluid flow.

From the past few years, the study regarding the implementation of hybrid nanofluid to improve heat transfer has been a hot topic in the fluid dynamics community. For instance, Devi and Devi [29] investigated the flow features past a stretching sheet considering Cu–Al_2O_3/water hybrid nanofluid. Here authors have introduced a new thermophysical model of hybrid nanofluid. In continuation of this work, Suresh et al. [30] verified and validated this thermophysical model with the experimental data. After that Devi and Devi [31] extended their work taking three-dimensional flow subject to the Newtonian heating condition. With their experiment, they came to the conclusion that the rate of heat transfer in case of hybrid nanofluid is much higher than that of regular nanofluid. Prakash and Devi [32] unfolded the impact of hydromagnetic hybrid Al_2O_3–Cu/water nanofluid flow over a slendering stretching sheet with prescribed surface temperature. Bahiraei and Mazaheri [33] discussed the applications of a novel hybrid nanofluid containing graphene–platinum nanoparticles in a chaotic twisted geometry for utilization in miniature devices. Aziz et al. [34] presented the outcomes of entropy generation due to Maxwell hybrid nanofluid flow under the influence of inclined magnetic field, thermal radiation and Joule heating. The flow characteristics of hybrid nanofluid flow through an exponentially stretching/shrinking sheet with mixed convection and Joule heating have been analysed by Yashkun et al. [35]. Sharma et al. [36] performed a numerical as well as statistical approach to study the nature of graphene Maxwell nanofluid flow past a linearly stretched sheet. Zhang et al. [37] portrayed the effects of graphite particles/Fe3+ on the properties of anoxic activated sludge. Other remarkable researches in this fields have been investigated by [38–40].

In view of industrial applications, one cannot ignore the features of surface heat transfer due to thermal radiation in various processes such as design of furnace, solar power technology, missiles devices, electrical power generation etc., that requires a very high temperature. At present, it is becoming a trend to depend more on renewable as well as sustainable energy sources by the industrial sectors rather than conventional energy sources. The major source of renewable energy is the solar energy whereas thermal radiation plays a significant role in converting the solar energy into the suitable form required by the industries. In this regard, some noteworthy research works are due to [41–46].

One point to note here that, in all the aforementioned literatures, the influence of viscous dissipation has not been considered but we must not forget that viscous dissipation plays a vital role in polymer manufacturing, food processing, lubrications,

instrumentations etc. Vajravelu and Hadjinicolaou [47] discussed the consequences of heat transfer in case of viscous fluid flow at stretching sheet considering the effect of viscous dissipation along with heat generation. Some other significant contributions in this regard are due to Partha et al. [48], Cortell [49] and El-Aziz [50], etc. Later this, various investigators namely Devi and Ganga [51] and Daniel et al. [52] framed their problems by taking into account of the mutual influence of both viscous and Joule dissipations. After this, Mukhopadhyay and Gorla [53] and Singh and Makinde [54] investigated the fluid flow model considering the case of partial slip under the impact of magnetic field.

The principal goal of the current investigation is to unfold the impact of thermal radiation and heat absorption as well as viscous and Joule dissipations on Maxwell hybrid (taking copper and graphene nanoparticles) nanofluid flow past a linearly varying stretched sheet which is kept horizontally under the condition of velocity slip. Shooting scheme is employed with the help of Runge–Kutta–Fehlberg technique to solve the highly non-linear governing flow equations numerically. Moreover, multiple regression estimation analysis has also been performed on the figures of local Nusselt number and wall velocity gradient. In the best of our knowledge, no such attempt has been made earlier although the fertility of thoughts and the phenomena explained in the present work can be expected to lead to extremely productive interactions across disciplines.

2. Development of our model

An electrically conducting, optically thick, unsteady two-dimensional flow of heat-absorbing Maxwell hybrid nanofluid past a linearly stretched sheet embedded in a porous medium has been considered. The hybrid nanofluid is manufactured by adding copper (Cu) nanoparticle into the ethylene glycol (base fluid) at a contact volume fraction (ϕ_1) then graphene nanoparticles are dispersed into the copper–ethylene glycol nanofluid to make it a hybrid nanofluid at volume fraction (ϕ_2). Table 1 portrays the thermophysical properties of the base fluid as well as the nanoparticles. The orientation of Cartesian coordinate system is chosen in such a way that the stretching sheet is aligned to x-axis while y-axis is perpendicular to it. The flow is constrained in the region $y > 0$. Fig. 1 represents the physical sketch of the coordinate system along with the flow configuration.

In order to carry out the present investigation, the following assumptions we have made:

- The sheet is being stretched with a time-dependent velocity $U_w(x,t) = cx(1-\alpha t)^{-1}$, where c and $(1-\alpha t)^{-1}$ (here $\alpha t < 1$) are the initial and effective stretching rates.
- Between the base fluid and the nanoparticles, there exist a state of thermal equilibrium.
- The size of nanoparticles is small as compared to the size of the pores.
- An unsteady magnetic field $B(t) = B_0(1-\alpha t)^{-1/2}$ is applied at an angle γ about the x-axis.
- Since the magnetic Reynolds number is chosen to be very small, the impact of magnetic field induced by the fluid flow is neglected [17].
- The influence of polarization is also ignored due to the absence of any externally applied electric field.
- The simultaneous effect of viscous as well as Joule dissipations have been taken into account.
- The wall temperature of the hybrid nanofluid is considered to be T_w while the temperature outside the boundary regime, known as free stream temperature, is denoted by T_∞.

Based on the above assumptions, the constitutive flow equations for conservation of mass, momentum and energy for the hybrid Maxwell nanofluid are given by [34,36,55]:

The equation of continuity:

$$\frac{\partial u}{\partial x} + \frac{\partial v}{\partial y} = 0. \tag{1}$$

The momentum equation:

$$\left(\frac{\partial}{\partial t} + u\frac{\partial}{\partial x} + v\frac{\partial}{\partial y}\right)u = \frac{\mu_{hnf}}{\rho_{hnf}}\left(\frac{\partial^2 u}{\partial y^2}\right) - \lambda\left(u^2\frac{\partial^2 u}{\partial x^2} + 2uv\frac{\partial^2 u}{\partial x \partial y} + v^2\frac{\partial^2 u}{\partial y^2}\right) - \frac{\sigma_{hnf}B^2(t)u}{\rho_{hnf}}\sin^2\gamma - \frac{\nu_{hnf}}{K}u. \tag{2}$$

The energy equation:

$$\left(\frac{\partial}{\partial t} + u\frac{\partial}{\partial x} + v\frac{\partial}{\partial y}\right)T = \frac{k_{hnf}}{(\rho C_p)_{hnf}}\left(\frac{\partial^2 T}{\partial y^2}\right) - \frac{1}{(\rho C_p)_{hnf}}\left[\frac{\partial q_r}{\partial y} + Q_0(T - T_\infty)\right] \frac{\sigma_{hnf}B^2(t)u^2}{(\rho C_p)_{hnf}}\sin^2\gamma + \frac{\mu_{hnf}}{(\rho C_p)_{hnf}}\left(\frac{\partial u}{\partial y}\right)^2. \tag{3}$$

The boundary conditions are

$$u = U_w + s\mu_{hnf}\left(\frac{\partial u}{\partial y}\right), \quad v = V_w, \quad -k_f\left(\frac{\partial T}{\partial y}\right) = h_f(T_w - T) \quad \text{at} \quad y = 0, \tag{4}$$

$$u \to 0, \quad T \to T_\infty \quad \text{as} \quad y \to \infty. \tag{5}$$

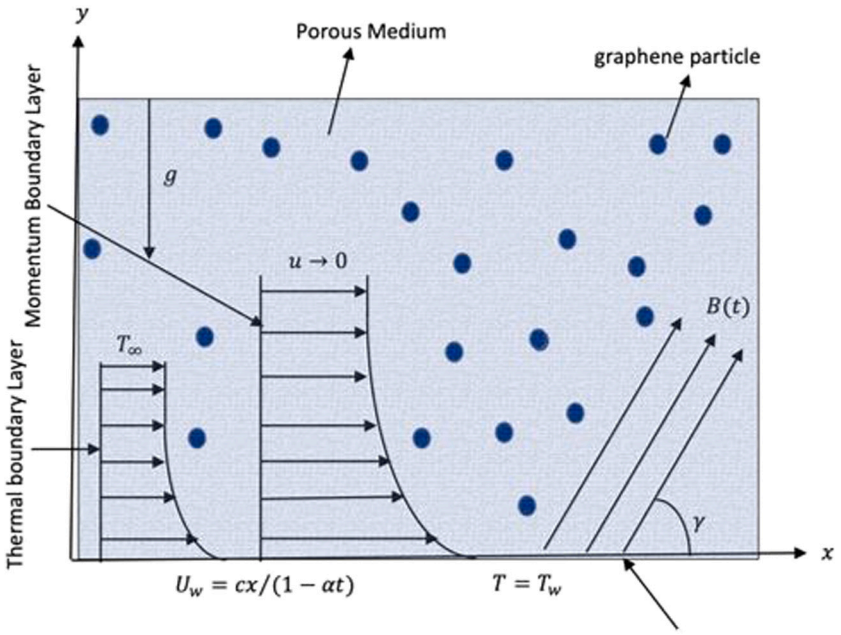

Fig. 1. Schematic diagram of the problem.

Table 1
Thermophysical properties of base fluid and nanoparticles [34,36].

Thermophysical properties	ρ (kg/m^3)	c_p (J/kg K)	k (W/mK)	σ (S/m)
Ethylene glycol	1114	2415	0.252	5.5×10^{-6}
Copper	8933	385	401	5.96×10^{7}
Graphene	2250	2100	2500	1×10^{7}

Here u and v are, respectively, the graphene Maxwell hybrid nanofluid velocities along x-direction and y-direction, t represents time. μ_{hnf}, ν_{hnf}, ρ_{hnf}, σ_{hnf}, k_{hnf} and $(\rho C_p)_{hnf}$ signify dynamic viscosity, kinematic viscosity, density, electrical conductivity, thermal conductivity and specific heat capacity of the hybrid nanofluid respectively. $\lambda = \lambda_0(1-\alpha t)$ denotes thermal relaxation, where λ_0 is the initial relaxation rate. $K = K_0(1-\alpha t)$ is the porosity parameter where K_0 represents the porosity at $t = 0$. T, q_r and Q_0 indicate, respectively, the temperature of the hybrid nanofluid, thermal radiation and heat absorption. $s = s_0\sqrt{(1-\alpha t)}$ is the velocity slip factor where s_0 is the initial slip at $t = 0$. V_w implies suction/injection for the hybrid nanofluid. The terms k_f and h_f signifies the thermal conductivity and heat transfer coefficient of the hybrid nanofluid respectively. The expressions of different thermophysical properties for both normal nanofluid and hybrid nanofluid are depicted in Table 2.

According to Rosseland approximation [56], for an optically thick radiative fluid, the expression for thermal radiation q_r is given by

$$q_r = -\frac{4\sigma^*}{3k^*}\frac{\partial T^4}{\partial y}, \tag{6}$$

where k^* represents absorption coefficient and $\sigma^*(= 5.67 \times 10^{-8}$ W/m^2 K$^4)$ denotes Stefan–Boltzmann constant.

3. Solution of the problem

Our chosen problem is comprised of a set of partial differential equations which are coupled in nature. Hence, to obtain an exact solution is quite challenging with the known techniques. That is why, with an aim to have a similar solution of the problem, the similarity variable $\eta = \sqrt{\frac{c}{\nu_f(1-\alpha t)}}y$, stream function $\psi = \sqrt{\frac{c\nu_f}{1-\alpha t}}xf(\eta)$ and non-dimensional temperature $\theta = \frac{T-T_\infty}{T_w-T_\infty}$ are introduced to convert the mathematical model into dimensionless forms.

Now in terms of stream function ψ, the velocity components of hybrid nanofluids u and v are defined by $u = \frac{\partial\psi}{\partial y}$ and $v = -\frac{\partial\psi}{\partial x}$, which satisfy the continuity Eq. (1).

Making use of above mentioned similarity transformations, the non-dimensional form of momentum Eq. (2) and energy Eq. (3) are given by

$$A\left(\frac{\eta}{2}f'' + f'\right) + f'^2 - ff'' - \frac{\phi_a}{\phi_b}\left(f''' + K_1 f'\right) + \beta\left(f^2 f''' - 2ff'f''\right) + \frac{\phi_e}{\phi_b}M\sin^2\gamma f' = 0, \tag{7}$$

Table 2
Thermophysical attributes of normal nanofluid and hybrid nanofluid [34,35].

Thermophysical properties	Normal nanofluid	Hybrid nanofluid
Density	$\rho_{nf} = (1-\phi_1)\rho_f + \phi_1\rho_{n_1}$	$\rho_{hnf} = (1-\phi_2)[(1-\phi_1)\rho_f + \phi_1\rho_{n_2}] + \phi_2\rho_{n_1}$
Heat capacity	$(\rho C_p)_{nf} = (1-\phi_1)(\rho C_p)_f + \phi_1(\rho C_p)_{n_1}$	$(\rho C_p)_{hnf} = (1-\phi_2)[(1-\phi_1)(\rho C_p)_f + \phi_1(\rho C_p)_{n_1}] + \phi_2(\rho C_p)_{n_2}$
Dynamic viscosity	$\mu_{nf} = \frac{\mu_f}{(1-\phi_1)^{2.5}}$	$\mu_{hnf} = \frac{\mu_f}{(1-\phi_1)^{2.5}(1-\phi_2)^{2.5}}$
Thermal conductivity	$k_{nf} = \frac{k_{n_1}+2k_f-2\phi_1(k_f-k_{n_1})}{k_{n_1}+2k_f+\phi_1(k_f-k_{n_1})} \times k_f$	$k_{hnf} = \frac{k_{n_2}+2k_{nf}-2\phi_2(k_{nf}-k_{n_2})}{k_{n_2}+2k_{nf}+\phi_2(k_{nf}-k_{n_2})} \times k_{nf}$
Electrical conductivity	$\sigma_{nf} = 1 + \frac{3\left(\frac{\sigma_{n_1}}{\sigma_f}-1\right)\phi_1}{2+\frac{\sigma_{n_1}}{\sigma_f}-\left(\frac{\sigma_{n_1}}{\sigma_f}-1\right)\phi_1} \times \sigma_f$	$\sigma_{hnf} = \frac{\sigma_{n_2}+2\sigma_{nf}-2\phi_2(\sigma_{nf}-\sigma_{n_2})}{\sigma_{n_2}+2\sigma_{nf}+\phi_2(\sigma_{nf}-\sigma_{n_2})} \times \sigma_{nf}$

$$\theta''\left(1+\frac{1}{\phi_d}\mathrm{Pr}Nr\right)+\mathrm{Pr}\frac{\phi_c}{\phi_d}\left(f\theta'-A\frac{\eta}{2}\theta'\right)+\frac{\mathrm{Pr}}{\phi_d}\left[\phi_e M\mathrm{Ecsin}^2\gamma f'^2-G\theta+\phi_a\mathrm{Ec}f''^2\right]=0. \tag{8}$$

The corresponding boundary conditions in the non-dimensional form become

$$f'(0)=1+\phi_a A_1 f''(0),\quad f(0)=S,\quad \theta'(0)=-\mathrm{Bi}\Big(1-\theta(0)\Big), \tag{9}$$

$$f'(\eta)\to 0,\quad \theta(\eta)\to 0\quad \text{as}\quad \eta\to\infty. \tag{10}$$

where $\phi_a=\frac{\mu_{hnf}}{\mu_f}$, $\phi_b=\frac{\rho_{hnf}}{\rho_f}$, $\phi_c=\frac{(\rho C_p)_{hnf}}{(\rho C_p)_f}$, $\phi_d=\frac{k_{hnf}}{k_f}$ and $\phi_e=\frac{\sigma_{hnf}}{\sigma_f}$. The primes stand for differentiation of function with respect to η. $A=\frac{\alpha}{c}$ is the unsteadiness parameter, $\beta=c\lambda_0$ is the Maxwell parameter, $M=\frac{\sigma_f B_0^2}{c\rho_f}$ indicates magnetic parameter, $K_1=\frac{\nu_f}{cK_0}$ denotes the porosity parameter, $\mathrm{Pr}=\frac{\nu_f}{\alpha_f}$ is the Prandtl number, $\alpha_f=\frac{k_f}{(\rho C_p)_f}$ is the thermal diffusivity parameter, $Nr=\frac{16}{3}\frac{\sigma^* T_\infty^3}{k^*\nu_f(\rho C_p)_f}$ is the radiation parameter, $G=\frac{Q_0(1-\alpha t)}{c(\rho C_p)_f}$ implies the heat absorption parameter, $\mathrm{Ec}=\frac{U_w^2}{(C_p)_f(T_w-T_\infty)}$ stands for local Eckert number, $A_1=s_0\sqrt{\frac{c}{\nu_f}}\mu_f$ is the velocity slip parameter, $S=-V_w\sqrt{\frac{1-\alpha t}{c\nu_f}}$ is the suction/injection parameter and $\mathrm{Bi}=\frac{h_f}{k_f}\sqrt{\frac{\nu_f(1-\alpha t)}{c}}$ denotes the Biot number.

4. Physical quantities of engineering interests

In view of engineering and practical applications, the exploration of some physical quantities i.e. the skin friction coefficient C_f and local Nusselt number Nu_x have enormous significance. These physical quantities are defined as [34].

$$C_f=\frac{\tau_w}{\rho_f U_w^2}\quad\text{and}\quad Nu_x=\frac{xq_w}{k_f(T_w-T_\infty)}, \tag{11}$$

where $\tau_w=\mu_{hnf}\left(\frac{\partial u}{\partial y}\right)_{y=0}$ denotes the wall skin friction and $q_w=-k_{hnf}\left(1+\frac{16}{3}\frac{\sigma^* T_\infty^3}{k^*\nu_f(\rho C_p)_f}\right)\left(\frac{\partial T}{\partial y}\right)_{y=0}$ indicates the wall heat flux.

Applying the dimensionless similarity transformations, we obtain

$$C_f Re_x^{1/2}=\phi_a f''(0)\quad\text{and}\quad Nu_x Re_x^{-1/2}=\phi_d(1+Nr)\theta'(0), \tag{12}$$

where $Re_x=\frac{U_w(x)}{\nu_f}$ is the local Reynolds number.

5. Implementation of numerical method

Due to complexity and highly nonlinearity of the mathematical model represented by Eqs. (7) and (8) along with the boundary conditions (9) and (10), it is not possible to solve those with the aid of analytical techniques. Therefore, we solved the system of equations by employing shooting technique with the help of Runge–Kutta–Fehlberg method (RKF45). In this technique, at first the Eqs. (7) and (8) are converted into five first order differential equations. After that, Runge–Kutta–Fehlberg method is executed to solve these sets of five differential equations. The detailed explanation of Shooting technique and Runge–Kutta–Fehlberg method are given below:

5.1. Shooting method

The Shooting method is technique for obtaining the solution of boundary value problem (BVP). In this technique, we are converting the given higher order boundary value problem into a system of first order initial value problem (IVP). In this technique, we choose the random value of one end of the initial value problem and try to get the solution at other end with the help of Runge–Kutta–Fhelburg method (RKF45) by taking suitable step-size h. If we are getting the solution at other end which is equal to given boundary value problem then our guess is correct otherwise, again make the guess with the help of Secant method and repeat the same process until we are not getting the desired solution at other end.

5.2. Runge–Kutta–Fehlberg method (RKF45)

One way to guarantee accuracy in the solution of an IVP is to solve the problem twice using step sizes h and $h/2$ and compare answers at the mesh points corresponding to the larger step size. But this requires a significant amount of computation for the smaller step size and must be repeated if it is determined that the agreement is not good enough.

The Runge–Kutta–Fehlberg method (denoted RKF45) is one way to try to resolve this problem. It has a procedure to determine if the proper step size h is being used. At each step, two different approximations for the solution are made and compared. If the two answers are in close agreement, the approximation is accepted. If the two answers do not agree to a specified accuracy, the step size is reduced. If the answers agree to more significant digits than required, the step size is increased.

Each step requires the use of the following six values:

$$
\begin{aligned}
k_1 &= hf\left(t_k,\ y_k\right),\\
k_2 &= hf\left(t_k + \frac{1}{4}h,\ y_k + \frac{1}{4}k_1\right),\\
k_3 &= hf\left(t_k + \frac{3}{8}h,\ y_k + \frac{3}{32}k_1 + \frac{9}{32}k_2\right),\\
k_4 &= hf\left(t_k + \frac{12}{13}h,\ y_k + \frac{1932}{2197}k_1 - \frac{7200}{2197}k_2 + \frac{7296}{2197}k_3\right),\\
k_5 &= hf\left(t_k + h,\ y_k + \frac{439}{216}k_1 - 8k_2 + \frac{3680}{513}k_3 - \frac{845}{4104}k_4\right),\\
k_6 &= hf\left(t_k + \frac{1}{2}h,\ y_k - \frac{8}{27}k_1 + 2k_2 - \frac{3544}{2565}k_3 + \frac{1859}{4104}k_4 - \frac{11}{40}k_5\right).
\end{aligned}
\tag{13}
$$

Then an approximation to the solution of the IVP is made using a Runge–Kutta method of order 4:

$$
y_{k+1} = y_k + \frac{25}{216}k_1 + \frac{1408}{2565}k_3 + \frac{2197}{4101}k_4 - \frac{1}{5}k_5, \tag{14}
$$

where the four function values f_1, f_3, f_4 and f_5 are used. Notice that f_2 is not used in formula (14). A better value for the solution is determined using a Runge–Kutta method of order 5:

$$
z_{k+1} = y_k + \frac{16}{135}k_1 + \frac{6656}{12825}k_3 + \frac{28561}{56430}k_4 - \frac{9}{50}k_5 + \frac{2}{55}k_6. \tag{15}
$$

The optimal step size sh can be determined by multiplying the scalar s times the current step size h. The scalar s is

$$
s = \left(\frac{\text{tol}\ h}{2|z_{k+1} - y_{k+1}|}\right)^{1/4} \approx 0.84\left(\frac{\text{tol}\ h}{|z_{k+1} - y_{k+1}|}\right)^{1/4} \tag{16}
$$

where tol is the specified error control tolerance.

The derivation of formula (16) can be found in advanced books on numerical analysis. It is important to learn that a fixed step size is not the best strategy even though it would give a nicer-appearing table of values. If values are needed that are not in the table, polynomial interpolation should be used.

6. Mesh independence analysis and validation of numerical solutions

With the perspective of validating the results obtained by us employing the numerical technique, we have made a comparison of the numerical values of local Nusselt number Nu_x with those of Asim et al. [34] and have presented the results in tabular form. This validation procedure has been conducted along with the mesh independency test. For this purpose, we have first set $K_1 = 0$ and $G = 0$ in order to make our mathematical model similar to Asim et al. [34]. In the next step we have computed the values of Nu_x for the variations of two parameters β and A with our developed code of Runge–Kutta–Fehlberg numerical technique by considering the thermophysical properties of ferro-copper (Fe_3O_4–Cu) nanoparticles (as chosen by Asim et al. [34]) instead of graphene nanoparticles. The developed code has been executed taking different element sizes and it was found that solution becomes independent of element size after taking the mesh (element) size smaller than 0.005 (Table 3). It is very clear from these comparisons that there is an outstanding agreement among the numerical solutions which justifies the accuracy and validity of our obtained numerical results.

7. Results and discussion

In order to establish and discuss the significance of various pertinent flow parameters on the hybrid nanofluid velocity as well as the hybrid nanofluid temperature some graphical and tabular representations are necessary. By implementing above mentioned numerical technique, we have prepared the graphs and tables. Throughout the numerical computations, the default values of the flow parameters have been chosen as $\text{Pr} = 5, M = 0.3, K_1 = 0.1, \gamma = \pi/4, \beta = 0.1, A = 0.1, S = 0.1, Nr = 0.2, \text{Ec} = 0.1, \text{Bi} = 0.1$ and $G = 0.2$ until and otherwise specified particularly. In the figures, no-slip condition $A_1 = 0$ is depicted by solid lines whereas dashed lines stand for the slip condition $A_1 \neq 0$.

Table 3
Comparison of the numerical values of local Nusselt number $(-Nu_x \mathrm{Re}_x^{1/2})$ for the variations in β and A.

β	A	Asim et al. [34]	Present result			
			$h = 0.05$	$h = 0.01$	$h = 0.005$	$h = 0.001$
0.01		0.0824	0.08278689	0.08258523	0.08258570	0.08258570
0.1	0.6	0.0819	0.08236297	0.08203496	0.08203498	0.08203498
0.3		0.0808	0.08102047	0.08083967	0.08083977	0.08083977
	0.6	0.0824	0.08278689	0.08258523	0.08258570	0.08258570
0.01	1.6	0.0879	0.08823968	0.08804172	0.08804185	0.08804185
	2.6	0.0899	0.09051023	0.08994563	0.08994581	0.08994581

Velocity profile

Figs. 2–7 display the behaviour of graphene Maxwell hybrid nanofluid velocity under the influence of magnetic parameter, porosity parameter, Maxwell parameter, magnetic field's inclination angle, Maxwell parameter, unsteadiness parameter and suction/injection parameter. In Fig. 2 we see that the nanofluid velocity decreases when there is an increment in parameter of magnetic field (M) due to both velocity slip $(A_1 = 0.4)$ and velocity no-slip $(A_1 = 0)$ conditions. The reason behind this phenomenon is that as the strength of magnetic field is gradually increased, a retarding body force named as Lorentz force is enhanced which has a tendency to oppose the fluid motion. As a result of which a downfall in hybrid nanofluid velocity is noticed. From Fig. 3 it is perceived that there is a decrement in the velocity profile whenever the permeability of porous medium (K_1) is intensified. This fact can be justified as an increment in the porosity parameter leads to the thickness of velocity boundary layer and consequently, the fluid flow slows down. Fig. 4 implies that an magnetic field's inclination angle (γ) causes a reduction in velocity of the hybrid nanofluid. The logic for this nature is that, M has tendency to decrease the velocity of Maxwell graphene hybrid nanofluid and the resistive force's strength is optimum whenever the direction of applied magnetic field is transverse to stretched surface. The optimized resistive force is known as Lorentz force which suppresses the motion of fluid. The intensification in (β) and (A) result in reduction in velocity of Maxwell graphene hybrid nanofluid, as portrayed in Figs. 5 and 6. At higher Deborah numbers, the material behaviour changes to increasingly dominated by elasticity, demonstrating solid like behaviour, thereby slowing down the flow velocity and increasing the temperature of the fluid. It is visible from Fig. 7 that intensification in (S) results in reduction in velocity of Maxwell graphene hybrid nanofluid as due to suction, momentum boundary stick very near to the sheet surface and as a result it spoil the flow momentum, which cause for the fall in fluid velocity. It can also be concluded from all above mentioned figures that hybrid nanofluid velocity in case of slip condition is lower than that of no-slip condition.

Temperature profile

It is elucidated from Fig. 8 that with an increment in radiation parameter (Nr), the temperature of the hybrid nanofluid gets improved. Actually, radiation tends to upsurge the conduction influence of fluid and as a result of which thickening of thermal boundary layer takes place and in turn fluid temperature gets reduced. One can notice through Fig. 9 that temperature of the nanofluid acts as an increasing function of the magnetic field's inclination angle (γ). It can be perceived by Fig. 10 that enhancing values of Eckert number (Ec) results in an augmentation in the temperature profile. This feature of Maxwell fluid with copper and graphene nanoparticle can be explained with the fact that Ec makes the relation between enthalpy and the kinetic energy and also the entire work gets complete in under the existence of viscosity while kinetic energy is transformed to internal energy. Therefore, viscous dissipation has a property to accelerate the fluid's temperature. Fig. 11 portrays that Biot number Bi causes an enhancement in the Maxwell graphene nanofluid temperature. This can be justified on the basis that the enhancement in Biot number causes an increment in the convective heat transfer at the surface and as a result of which, temperature is getting enhanced. Fig. 12 implies that, due to increase in unsteadiness parameter (A), the temperature of Maxwell hybrid nanofluid gets risen. Fig. 13 implies that, because of enhancement in heat absorption parameter (G), a reduction in temperature profile is perceived. As G increases, absorbing capacity of heat from the fluid is enhancing and consequently, there is fall in fluid temperature. Further, it is to be noticed from Figs. 8–13 that under the condition with slip, the nanofluid temperature is lower than that of condition of without slip.

Variation of skin friction coefficient and Nusselt number

Due to real application view point, we have also presented the numerical values of wall gradient and heat transfer's rate in tabular form via Tables 4 and 5 for various values of regulatory flow parameters. For this, we have considered $\mathrm{Pr} = 5, M = 0.3, K_1 = 0.1, \gamma = \pi/4, \beta = 0.1, A = 0.1, S = 0.1, Nr = 0.2, \mathrm{Ec} = 0.1, \mathrm{Bi} = 0.1$ and $G = 0.2$. There values are kept unchanged while other values keep changing on computation process. It is visible from Table 4 that coefficient of skin friction under both with slip and without slip situations is enhanced because of enhancement due to unsteadiness parameter, Maxwell parameter, magnetic field, porosity parameter, magnetic field's inclination and suction parameter. Table 5 presents that rate of heat transfer (Nusselt number) is enhanced due to positive change in radiation parameter, viscous dissipation, Biot number, unsteadiness parameter, magnetic field' inclination while it is reduced due to an increment in heat absorption parameter.

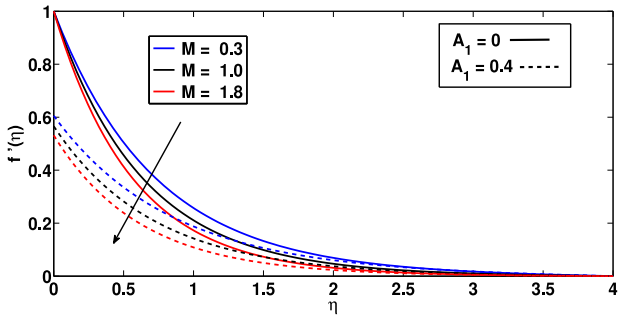

Fig. 2. Velocity profile due to variation in magnetic parameter M for both slip and no-slip conditions.

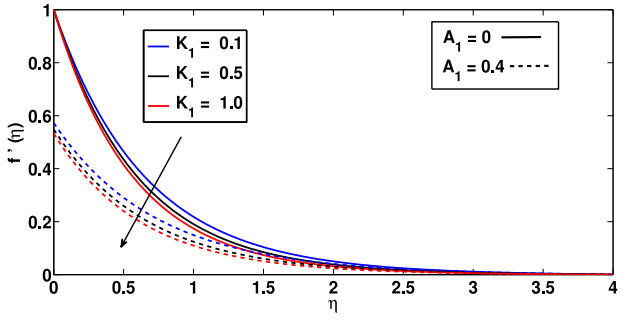

Fig. 3. Velocity profile due to variation in unsteadiness parameter K_1 for both slip and no-slip conditions.

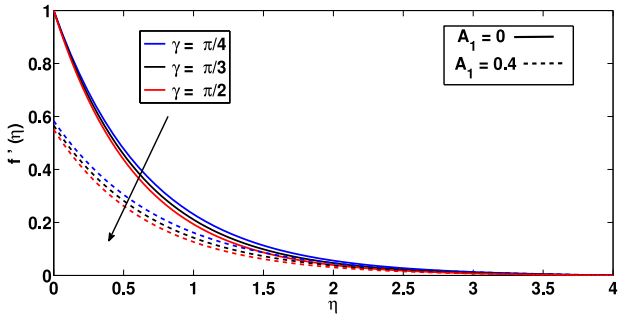

Fig. 4. Velocity profile due to variation in angle of inclination of magnetic field γ for both slip and no-slip conditions.

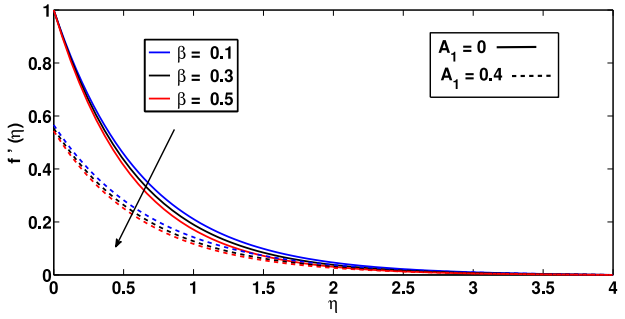

Fig. 5. Velocity profile due to variation in Maxwell parameter β for both slip and no-slip conditions.

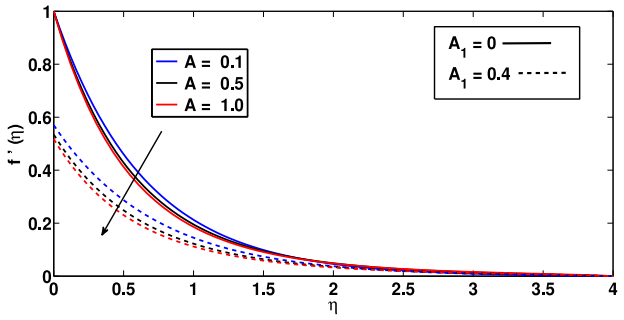

Fig. 6. Velocity profile due to variation in unsteadiness parameter A for both slip and no-slip conditions.

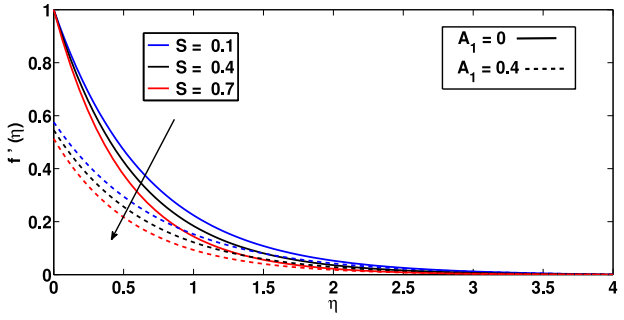

Fig. 7. Velocity profile due to variation in suction/injection parameter S for both slip and no-slip conditions.

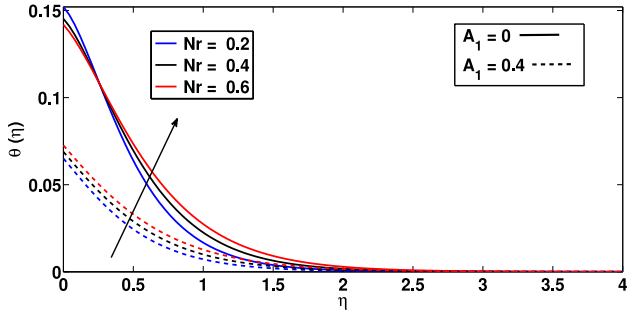

Fig. 8. Temperature profile due to variation in radiation parameter Nr for both slip and no-slip conditions.

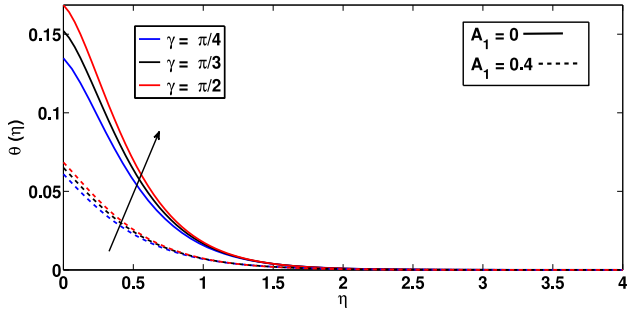

Fig. 9. Temperature profile due to variation in angle of inclination of magnetic field γ for both slip and no-slip conditions.

8. Multiple regression analysis: Analysis of both Nusselt number and coefficient of skin friction

We did statistical approach for the multiple quadratic regression analysis to get an overview of the relationship between two or more physical parameters. In this segment, we did the multiple quadratic regression estimation analysis for Nusselt number and

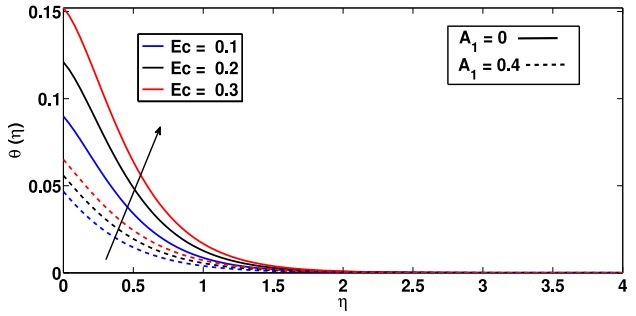

Fig. 10. Temperature profile due to variation in Eckert number Ec for both slip and no-slip conditions.

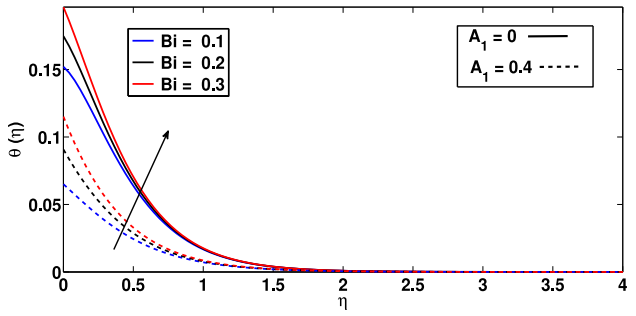

Fig. 11. Temperature profile due to variation in Biot number Bi for both slip and no-slip conditions.

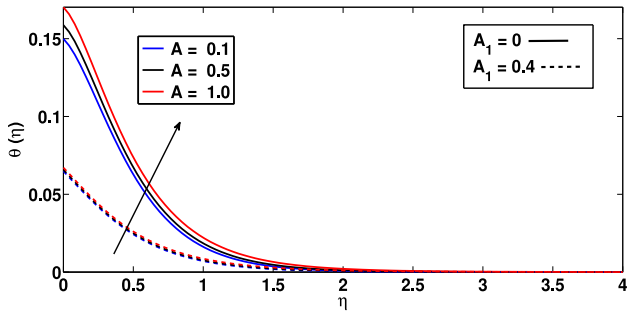

Fig. 12. Temperature profile due to variation in unsteadiness parameter A for both slip and no-slip conditions.

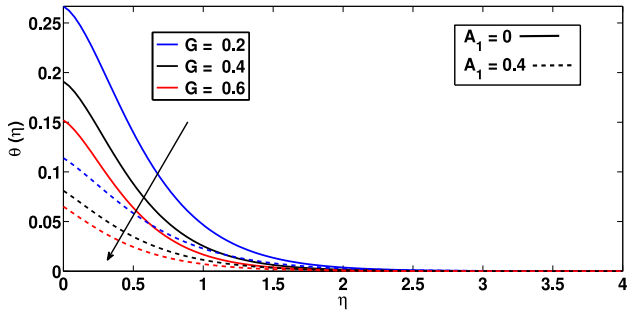

Fig. 13. Temperature profile due to variation in heat absorption parameter G for both slip and no-slip conditions.

skin friction coefficient. The regression estimation of skin friction coefficient is written for 125 various values of K_1 and M, taken randomly within the intervals [0.1, 0.5] and [1, 7] respectively for two different values of *beta* i.e., $\beta = 0.1$ and $\beta = 0.5$. Similarly, multiple quadratic regression estimation of Nusselt number is written for 135 various values of Nr and Ec, taken randomly within

Table 4
Variation of skin friction coefficient ($C_f \mathrm{Re}_x^{1/2}$) under both no-slip ($A_1 = 0$) and slip ($A_1 = 0.4$) conditions.

Flow parameters						$-C_f \mathrm{Re}_x^{1/2}$ (Skin friction coefficient)	
A	β	M	K_1	γ	S	$A_1 = 0$	$A_1 = 0.4$
0.1						2.119119	1.074128
0.5	0.1	1	0.2	$\pi/3$	0.2	2.245460	1.116515
1.0						2.396955	1.163965
	0.1					2.151116	1.085115
0.2	0.3	1	0.2	$\pi/3$	0.2	2.264423	1.101748
	0.5					2.380236	1.117955
		0.3				1.877803	0.986543
0.2	0.1	1	0.2	$\pi/3$	0.2	2.151116	1.085115
		1.8				2.423517	1.170927
			0.1			2.103521	1.068919
0.2	0.3	1	0.5	$\pi/3$	0.2	2.287521	1.129487
			0.8			2.415685	1.168611
				$\pi/4$		2.025930	1.041667
0.2		1	0.2	$\pi/3$	0.2	2.151116	1.085115
				$\pi/2$		2.268901	1.123601
					0.1	2.065655	1.061107
0.2	2	1	0.2	$\pi/3$	0.4	2.340535	1.135533
					0.7	2.681634	1.217680

Table 5
Variation of Nusselt number ($Nu_x \mathrm{Re}_x^{1/2}$) under both no-slip ($A_1 = 0$) and slip ($A_1 = 0.4$) conditions.

Flow parameters						$-Nu_x \mathrm{Re}_x^{1/2}$ (Nusselt number)	
Nr	G	Ec	Bi	A	γ	$A_1 = 0$	$A_1 = 0.4$
0.2						0.153773	0.065753
0.4	3	0.2	0.1	0.2	$\pi/3$	0.171339	0.081228
0.6						0.191230	0.097837
	1					0.269744	0.115214
0.2	2	0.2	0.1	0.2	$\pi/3$	0.193026	0.081940
	3					0.153773	0.065753
		0.1				0.090806	0.047191
0.2	3	0.2	0.1	0.2	$\pi/3$	0.153773	0.065753
		0.3				0.216740	0.084314
			0.1			0.153773	0.065753
0.2	3	0.2	0.2	0.2	$\pi/3$	0.176746	0.091783
			0.3			0.198521	0.116419
				0.1		0.151586	0.065517
0.2	3	0.2	0.1	0.5	$\pi/3$	0.160498	0.066503
				1.0		0.172148	0.067861
					$\pi/4$	0.136232	0.061635
0.2	3	0.2	0.1	0.2	$\pi/3$	0.153773	0.065753
					$\pi/3$	0.170475	0.069213

the intervals [0.2, 0.6] and [0.1, 0.3] respectively for two separate values of Pr i.e., Pr = 5 and Pr = 10. Remaining parameters are kept fixed, during the process of estimation which is mentioned in Section 7. The model of estimated quadratic regression for $C_f Re_x^{1/2}$ due to changing values of K_1 and M are as follows:

$$Cf_{est} = C_f + b_1 M + b_2 K_1 + b_3 M^2 + b_4 K_1^2 + b_5 M K_1, \tag{17}$$

whereas the model of estimated quadratic regression for $Nu_x Re_x^{1/2}$ due to changing values of Ec and thermal radiation parameters are provided as:

$$Nu_{est} = Nu + c_1 \mathrm{Ec} + c_2 Nr + c_3 \mathrm{Ec}^2 + c_4 Nr^2 + c_5 \mathrm{Ec} Nr. \tag{18}$$

Tables 6 and 7 illustrate the coefficients of multiple quadratic regression estimated for various values of coefficient of skin friction coefficient and Nusselt number due to variation in different parameters. The largest error bound for Nusselt number $\varepsilon_1 = (Nu_{est} - Nu)/Nu$ and for skin friction $\varepsilon = (Cf_{est} - C_f)/C_f$ are also provided in above tables. It is evident from these tabular numeric values that porous medium parameter's coefficient is larger than magnetic field parameter's coefficient which explores the findings that coefficient of skin friction is higher sensitive for changing in K_1 than M for given two values of β. Similarly, we can notice that Nusselt number is high sensitive for Nr than Ec.

Table 6
The numerical values of $C_f Re_x^{1/2}$ and error bound for different values of M and K_1.

β	Cf	b_1	b_2	b_3	b_4	b_5	ϵ
0.1	−0.9224	−0.2182	−0.3293	0.0073	0.0376	0.0227	0.0058
0.5	−0.9153	−0.2169	−0.3190	0.0070	0.0476	0.0187	0.0060

Table 7
The numerical values of $Nu_x Re_x^{1/2}$ and error bound for different values of Ec and Nr.

Pr	Nu	c_1	c_2	c_3	c_4	c_5	ϵ_1
5	−3.0416	1.2816	−2.6638	−0.1796	1.0634	1.1216	0.000001064
10	−4.0875	1.9619	−4.0412	0.0702	2.0579	1.5836	0.000026918

9. Final outcomes

Noteworthy findings of the present investigation can be summarized as follows: Because of intensification of the angle at which magnetic field is inclined, unsteadiness parameter, magnetic field, permeability of porous medium, suction parameter and maxwell parameter, velocity of graphene Maxwell hybrid nanofluid is reduced. In the regime of boundary layer region, graphene Maxwell hybrid nanofluid's temperature is getting enhanced for rising the values of magnetic field's inclination angle, radiation, unsteadiness parameters, Biot number and viscous dissipation whereas a reverse trend is visible for heat absorption parameter. Wall gradient at stretching sheet increases significantly for Magnetic field, porosity, unsteadiness parameter, Maxwell parameter, suction/injection parameter and angle at which magnetic field is inclined. Radiation, viscous dissipation, Biot number, unsteadiness parameter and inclination angle of magnetic field tend to enhance heat transfer rate of nanofluid whereas opposite behaviour of heat transfer rate is noticed because of augmentation in heat absorption parameter. Moreover, while performing regression analysis, it is notable that wall gradient is less sensitive to magnetic field effect compared to porous medium permeability whereas heat transfer rate is less sensitive to viscous dissipation compared to thermal radiation.

Declaration of competing interest

The authors declare that they have no known competing financial interests or personal relationships that could have appeared to influence the work reported in this paper.

Acknowledgement

Dr. Rohit Sharma is grateful to the University Grants Commission New Delhi, Government of India for providing support to this research work under the research project No. F. 30 457/2018 (BSR).

References

[1] S.U.S. Choi, J.A. Eastman, Enhancing Thermal Conductivity of Fluids with Nanoparticles, Tech. Rep., Argonne National Lab., IL (United States), 1995.
[2] J.A. Eastman, S.U.S. Choi, S. Li, W. Yu, L. Thompson, Anomalously increased effective thermal conductivities of ethylene glycol-based nanofluids containing copper nanoparticles, Appl. Phys. Lett. 78 (6) (2001) 718–720.
[3] S. Rashidi, O. Mahian, E.M. Languri, Applications of nanofluids in condensing and evaporating systems, J. Therm. Anal. Calorim. 131 (3) (2018) 2027–2039.
[4] K. Das, T. Chakraborty, P.K. Kundu, Lie group transformation for double-diffusive free convection nanofluid flow over an inclined plane, Proc. Natl. Acad. Sci., India Sect. A: Phys. Sci. 89 (2) (2019) 387–396.
[5] G.S. Seth, R. Kumar, A. Bhattacharyya, Entropy generation of dissipative flow of carbon nanotubes in rotating frame with Darcy-Forchheimer porous medium: A numerical study, J. Mol. Liq. 268 (2018) 637–646.
[6] S. Nadeem, M.R. Khan, A.U. Khan, MHD stagnation point flow of viscous nanofluid over a curved surface, Phys. Scr. 94 (11) (2019) 115207.
[7] P. Ram, V.K. Joshi, V. Kumar, S. Sharma, Rheological effects due to oscillating field on time dependent boundary layer flow of magnetic nanofluid over a rotating disk, Proc. Natl. Acad. Sci., India Sect. A: Phys. Sci. 89 (2) (2019) 367–375.
[8] S. Rana, M. Nawaz, Investigation of enhancement of heat transfer in Sutterby nanofluid using Koo–Kleinstreuer and Li (KKL) correlations and cattaneo–christov heat flux model, Phys. Scr. 94 (11) (2019) 115213.
[9] Y. Ma, R. Mohebbi, M.M. Rashidi, Z. Yang, Y. Fang, Baffle and geometry effects on nanofluid forced convection over forward-and backward-facing steps channel by means of lattice Boltzmann method, Phys. A: Stat. Mech. Appl. 554 (2020) 124696.
[10] X. Xu, Y. Yang, L. Chen, X. Chen, T. Wu, Y. Li, X. Liu, Y. Zhang, B. Li, Optomechanical wagon-wheel effects for bidirectional sorting of dielectric nanoparticles, Laser Photonics Rev. 15 (6) (2021) 2000546.
[11] X. Zhang, Y. Zhang, Experimental study on enhanced heat transfer and flow performance of magnetic nanofluids under alternating magnetic field, Int. J. Therm. Sci. 164 (2021) 106897.
[12] A.H.C. Neto, F. Guinea, N.M.R. Peres, K.S. Novoselov, A.K. Geim, The electronic properties of graphene, Rev. Mod. Phys. 81 (1) (2009) 109.
[13] C. Chung, Y.-K. Kim, D. Shin, S.-R. Ryoo, B.H. Hong, D.-H. Min, Biomedical applications of graphene and graphene oxide, Acc. Chem. Res. 46 (10) (2013) 2211–2224.
[14] S. Mamatha Upadhya, M. Mahesha, C.S.K. Raju, Unsteady flow of carreau fluid in a suspension of dust and graphene nanoparticles with Cattaneo–Christov heat flux, J. Heat Transfer 140 (9) (2018).
[15] H.B. Santhosh, C.S.K. Raju, et al., Unsteady carreau radiated flow in a deformation of graphene nanoparticles with heat generation and convective conditions, J. Nanofluids 7 (6) (2018) 1130–1137.

[16] J.A. Shercliff, Textbook of Magnetohydrodynamics, Pergamon Press, Oxford-New York, 1965.
[17] R. Cramer, S. Pai, Magnetofluid Dynamics for Engineers and Applied Physicists, McGraw-Hill Book Company, New York, 1973.
[18] Y. Wang, C. Li, Y. Zhang, M. Yang, B. Li, D. Jia, Y. Hou, C. Mao, Experimental evaluation of the lubrication properties of the wheel/workpiece interface in minimum quantity lubrication (MQL) grinding using different types of vegetable oils, J. Clean. Prod. 127 (2016) 487–499.
[19] M. Ghalambaz, T. Groşan, I. Pop, Mixed convection boundary layer flow and heat transfer over a vertical plate embedded in a porous medium filled with a suspension of nano-encapsulated phase change materials, J. Mol. Liq. 293 (2019) 111432.
[20] M. Yang, C. Li, Y. Zhang, D. Jia, X. Zhang, Y. Hou, R. Li, J. Wang, Maximum undeformed equivalent chip thickness for ductile-brittle transition of zirconia ceramics under different lubrication conditions, Int. J. Mach. Tools Manuf. 122 (2017) 55–65.
[21] S. Barış, M.S. Dokuz, Three-dimensional stagnation point flow of a second grade fluid towards a moving plate, Internat. J. Engrg. Sci. 44 (1–2) (2006) 49–58.
[22] M.H. Haroun, Effect of deborah number and phase difference on peristaltic transport of a third-order fluid in an asymmetric channel, Commun. Nonlinear Sci. Numer. Simul. 12 (8) (2007) 1464–1480.
[23] M. Sajid, T. Hayat, S. Asghar, Non-similar analytic solution for MHD flow and heat transfer in a third-order fluid over a stretching sheet, Int. J. Heat Mass Transfer 50 (9–10) (2007) 1723–1736.
[24] T. Hayat, S. Noreen, M. Sajid, Heat transfer analysis of the steady flow of a fourth grade fluid, Int. J. Therm. Sci. 47 (5) (2008) 591–599.
[25] T. Hayat, A.M. Siddiqui, S. Asghar, Some simple flows of an Oldroyd-B fluid, Internat. J. Engrg. Sci. 39 (2) (2001) 135–147.
[26] C. Fetecau, C. Fetecau, A new exact solution for the flow of a Maxwell fluid past an infinite plate, Int. J. Non-Linear Mech. 38 (3) (2003) 423–427.
[27] Y. Wang, T. Hayat, Fluctuating flow of a Maxwell fluid past a porous plate with variable suction, Nonlinear Anal. RWA 9 (4) (2008) 1269–1282.
[28] M. Heyhat, N. Khabazi, Non-isothermal flow of Maxwell fluids above fixed flat plates under the influence of a transverse magnetic field, Proc. Inst. Mech. Eng., Part C: J. Mech. Eng. Sci. 225 (4) (2011) 909–916.
[29] S.P.A. Devi, S.S.U. Devi, Numerical investigation of hydromagnetic hybrid Cu–Al2O3/water nanofluid flow over a permeable stretching sheet with suction, Int. J. Nonlinear Sci. Numer. Simul. 17 (5) (2016) 249–257.
[30] S. Suresh, K. Venkitaraj, P. Selvakumar, M. Chandrasekar, Synthesis of Al2O3–Cu/water hybrid nanofluids using two step method and its thermo physical properties, Colloids Surf. A 388 (1–3) (2011) 41–48.
[31] S.S.U. Devi, S.P.A. Devi, Numerical investigation of three-dimensional hybrid Cu–Al2O3/water nanofluid flow over a stretching sheet with effecting Lorentz force subject to Newtonian heating, Canad. J. Phys. 94 (5) (2016) 490–496.
[32] M. Prakash, S. Devi, Hydromagnetic hybrid Al2O3-Cu/water nanofluid flow over a slendering stretching sheet with prescribed surface temperature, Asian J. Res. Soc. Sci. Humanit. 6 (9) (2016) 1921–1936.
[33] M. Bahiraei, N. Mazaheri, Application of a novel hybrid nanofluid containing graphene–platinum nanoparticles in a chaotic twisted geometry for utilization in miniature devices: thermal and energy efficiency considerations, Int. J. Mech. Sci. 138 (2018) 337–349.
[34] A. Aziz, W. Jamshed, Y. Ali, M. Shams, Heat transfer and entropy analysis of Maxwell hybrid nanofluid including effects of inclined magnetic field, Joule heating and thermal radiation, Discrete Contin. Dyn. Syst. Ser. A 13 (10) (2020) 2667.
[35] U. Yashkun, K. Zaimi, A. Ishak, I. Pop, R. Sidaoui, Hybrid nanofluid flow through an exponentially stretching/shrinking sheet with mixed convection and Joule heating, Int. J. Numer. Methods Heat Fluid Flow (2020).
[36] R. Sharma, S.M. Hussain, C.S.K. Raju, G.S. Seth, A.J. Chamkha, Study of graphene Maxwell nanofluid flow past a linearly stretched sheet: A numerical and statistical approach, Chinese. J. Phys. 68 (2020) 671–683.
[37] M. Zhang, L. Zhang, S. Tian, X. Zhang, J. Guo, X. Guan, P. Xu, Effects of graphite particles/Fe3+ on the properties of anoxic activated sludge, Chemosphere 253 (2020) 126638.
[38] X. Zhang, Y. Tang, F. Zhang, C.-S. Lee, A novel aluminum–graphite dual-ion battery, Adv. Energy Mater. 6 (11) (2016) 1502588.
[39] K. Yang, Q. Liu, Y. Zheng, H. Yin, S. Zhang, Y. Tang, Locally ordered graphitized carbon cathodes for high-capacity dual-ion batteries, Angew. Chem. 133 (12) (2021) 6396–6402.
[40] X. Wang, S. Handschuh-Wang, Y. Xu, L. Xiang, Z. Zhou, T. Wang, Y. Tang, Hierarchical micro/nanostructured diamond gradient surface for controlled water transport and fog collection, Adv. Mater. Interfaces (2021) 2100196.
[41] M. Sajid, T. Hayat, Influence of thermal radiation on the boundary layer flow due to an exponentially stretching sheet, Int. Commun. Heat Mass Transf. 35 (3) (2008) 347–356.
[42] X. Xu, M. Nieto-Vesperinas, Azimuthal imaginary poynting momentum density, Phys. Rev. Lett. 123 (23) (2019) 233902.
[43] M.M. Gulzar, A. Aslam, M. Waqas, M.A. Javed, K. Hosseinzadeh, A nonlinear mathematical analysis for magneto-hyperbolic-tangent liquid featuring simultaneous aspects of magnetic field, heat source and thermal stratification, Appl. Nanosci. 10 (12) (2020) 4513–4518.
[44] R. Kumar, A. Bhattacharyya, G.S. Seth, A.J. Chamkha, Transportation of magnetite nanofluid flow and heat transfer over a rotating porous disk with arrhenius activation energy: Fourth order noumerov's method, Chinese J. Phys. 69 (2021) 172–185.
[45] A. Bhattacharyya, R. Kumar, G.S. Seth, Capturing the features of peristaltic transport of a chemically reacting couple stress fluid through an inclined asymmetric channel with dufour and soret effects in presence of inclined magnetic field, Indian J. Phys. (2021) 1–18.
[46] Y. Zhang, C. Li, D. Jia, D. Zhang, X. Zhang, Experimental evaluation of MoS2 nanoparticles in jet MQL grinding with different types of vegetable oil as base oil, J. Clean. Prod. 87 (2015) 930–940.
[47] K. Vajravelu, A. Hadjinicolaou, Heat transfer in a viscous fluid over a stretching sheet with viscous dissipation and internal heat generation, Int. Commun. Heat Mass Transf. 20 (3) (1993) 417–430.
[48] M.K. Partha, P.V.S.N. Murthy, G.P. Rajasekhar, Effect of viscous dissipation on the mixed convection heat transfer from an exponentially stretching surface, Heat Mass Transf. 41 (4) (2005) 360–366.
[49] R. Cortell, Effects of viscous dissipation and radiation on the thermal boundary layer over a nonlinearly stretching sheet, Phys. Lett. A 372 (5) (2008) 631–636.
[50] M. Abd El-Aziz, Viscous dissipation effect on mixed convection flow of a micropolar fluid over an exponentially stretching sheet, Canad. J. Phys. 87 (4) (2009) 359–368.
[51] S.P.A. Devi, B. Ganga, Effects of viscous and joules dissipation on MHD flow, heat and mass transfer past a stretching porous surface embedded in a porous medium, Nonlinear Anal.: Model. Control 14 (3) (2009) 303–314.
[52] Y.S. Daniel, Z.A. Aziz, Z. Ismail, F. Salah, Effects of thermal radiation, viscous and joule heating on electrical MHD nanofluid with double stratification, Chinese J. Phys. 55 (3) (2017) 630–651.
[53] S. Mukhopadhyay, R.S.R. Gorla, Effects of partial slip on boundary layer flow past a permeable exponential stretching sheet in presence of thermal radiation, Heat Mass Transf. 48 (10) (2012) 1773–1781.
[54] G. Singh, O.D. Makinde, Mixed convection slip flow with temperature jump along a moving plate in presence of free stream, Therm. Sci. 19 (1) (2015) 119–128.
[55] H. Khan, M. Haneef, Z. Shah, S. Islam, W. Khan, S. Muhammad, The combined magneto hydrodynamic and electric field effect on an unsteady Maxwell nanofluid flow over a stretching surface under the influence of variable heat and thermal radiation, Appl. Sci. 8 (2) (2018) 160.
[56] M.Q. Brewster, Thermal Radiative Transfer and Properties, John Wiley and Sons, New York, 1992.